ACS Sustainable Chemistry & Engineering

Research Article

pubs.acs.org/journal/ascecg

Biomimetic Nanowire Structured Hydrogels as Highly Active and Recyclable Catalyst Carriers

Qian Mao, Shengjie Shi, and Huiliang Wang*

Beijing Key Laboratory of Energy Conversion and Storage Materials, College of Chemistry, Beijing Normal University, 19 Xinjiekouwai Street, Beijing 100875, People's Republic of China

Supporting Information

ABSTRACT: Nanowire hydrogels with high specific surface areas have great promise in many practical applications. However, the preparation of nanowire hydrogels using common materials and inexpensive means remains an outstanding challenge. This paper reports a novel method for creating aligned nanowire structured hydrogels by directional freezing and γ-radiation initiated polymerization of 2-hydroxyethyl methacrylate (HEMA) using *t*-butyl alcohol (TBA) as the solvent. The hydrogels prepared at a monomer concentration lower than 2.0 mol L^{-1} and a freezing rate higher than 10 mm min^{-1} are structured of nanowires, mimicking the microstructure of jellyfish mesogloea. Silver (Ag) nanoparticles (NPs) are introduced into the hydrogels with a chemical reduction method, and the Ag NPs are formed and deposited on the nanowires. Both size and content of Ag NPs in the hydrogels increase with increasing $AgNO_3$ concentration. The PHEMA and PHEMA/Ag nanocomposite hydrogels all possess very good compressive properties, and the composite hydrogels show higher compressive strengths and excellent deformation recovery. The PHEMA/Ag NPs composite hydrogels show excellent catalytic activity and reusability for the conversion of *o*-nitroaniline to 1,2-benzenediamine, with an apparent rate constant (k_{app}) up to 0.165 min^{-1}. This facile and efficient method can be applied to fabricate more nanowire hydrogels for many practical applications.

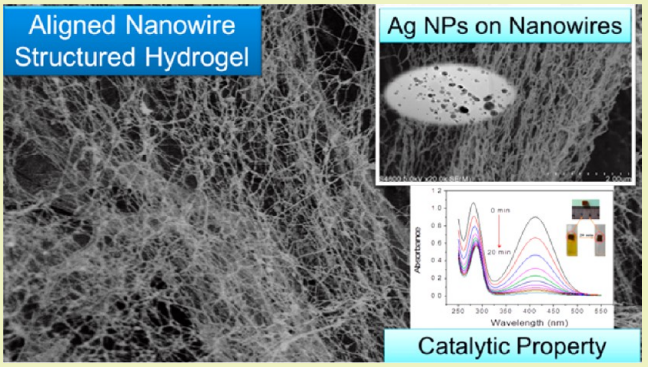

KEYWORDS: *Hydrogels, Nanowires, Jellyfish mesoglea, Silver nanoparticles, Directional freezing, Radiation-induced polymerization*

INTRODUCTION

Hydrogels are three-dimensional cross-linked hydrophilic polymeric networks that can swell largely rather than be dissolved in water. Benefiting from their porous microstructure and excellent biocompatibility, hydrogels have found many practical applications in biomedical, industrial and other fields.[1,2] Generally, common synthetic hydrogels in the freeze-dried state show porous structures consisted of micro- or sub-micro- sized pores with continuous and dense pore walls, which impede the fast diffusion and hence the exchange of substances between the hydrogels and the environment. This drawback can be overcome by modifying the microstructures of hydrogels. In recent years, several strategies have been developed to prepare hydrogels with different morphologies, such as macropores,[3,4] aligned porous structures,[5,6] hierarchical porous structure,[7] nanowires[8,9] and so on.

Porous hydrogels constructed of or containing nanowires have great promise in catalytic conversion,[10] selective absorption,[11] chemical connectors[9] and so on, as the nanowires with high specific surface areas provide more active sites for fulfilling their functionalities. Our recent study shows that jellyfish mesoglea, a biological hydrogel, is mainly composed of nanowires connected by nanosheets, forming a unique anisotropic macroporous microstructure that imparts jellyfish mesoglea with high mechanical strengths even at an extremely high water content of 97−99%.[12,13] Jellyfish mesoglea can be used as a matrix for the synthesis of extremely high content silver dendrites with high catalytic activity.[14] Unfortunately, most of the normal synthetic nanowires are inorganic components, such as silicon, manganese oxide, titania and cobalt oxide.[8,15−17] Only a few polymeric nanowire hydrogels have been reported, and the nanowires are usually made by complex and time-consuming methods, such as electrospining,[10] self-assembly[18] and more often template polymerization.[15,19] The preparation of nanowire hydrogels using common materials and inexpensive means remains an outstanding challenge.

Directional freezing has been used for fabricating hydrogels with aligned porous structures. However, only a few polymers that can form strong intermolecular hydrogen bonding (e.g., poly(vinyl alcohol))[20−22] can be used as the raw materials for directional freezing method. As an important progress of the directional freezing method, the combination of directional freezing and the polymerization of monomeric molecules in the

Received: January 29, 2015
Revised: July 17, 2015
Published: July 23, 2015

DOI: 10.1021/acssuschemeng.5b00482
ACS Sustainable Chem. Eng. 2015, 3, 1915−1924

frozen state has dramatically broadened the choice of raw materials.[5,23,24] The microstructure of the hydrogels can be tuned by the proper choice of freezing conditions (i.e., temperature and rate) as well as the monomer(s) and the solvent(s). The crystalline structures of the solvent(s) largely determine the microstructures of the hydrogels, as the gaps among the solvent crystals, formed by the phase separation during DF process, act as the templates for the polymerization of monomers. Water is the most commonly used solvent, and some organic solvents such as camphene, dioxane, cyclohexane, or cosolvents of *t*-butyl alcohol (TBA) and water are also used.[9,25,26] TBA has been widely applied in lyophilization, due to its high vapor pressure, low toxicity and low cost.[27−29] Fabietti and Trivedi reported the transition of TBA crystals from a planar interface to cellular and needle morphologies with increasing freezing velocity.[30] We presume that when TBA is used as the solvent, it could form many fine needle-like crystals under proper DF conditions, and hence forming many monomer-rich micro- or nanosized gaps, which transform into polymer wires after the polymerization in the frozen state. Therefore, nanowire structured hydrogels might be obtained.

In this work, we successfully prepared PHEMA nanowire hydrogels by the directional freezing and γ-radiation initiated polymerization of HEMA in TBA. The optimal conditions for synthesizing nanowire hydrogels were determined by varying the freezing rates and monomer concentrations. In addition, Ag nanoparticles (NPs) were introduced into the hydrogels and the catalytic activity of the PHEMA/Ag nanocomposite hydrogels was evaluated by catalyzing the reduction reaction of *o*-nitroaniline to 1,2-benzenediamine.

EXPERIMENTAL SECTION

Materials. 2-Hydroxyethyl methacrylate (HEMA, 98.0%) was purchased from Aladdin Reagent Database Inc. (Shanghai, China), silver nitrate ($AgNO_3$, AR grade), *o*-nitroaniline and sodium borohydride ($NaBH_4$, AR grade) were purchased from Beijing HWRK Chem Co., Ltd. (Beijing, China), and *t*-butyl alcohol (TBA, CP grade) was purchased from Tianjin Bodi Chem Co., Ltd. (Tianjin, China). All chemicals were used without futher purification.

PHEMA Hydrogel Preparation. HEMA solutions with the monomer concentrations of 1.5, 2.0, 2.5 and 3.0 mol L^{-1} using TBA as the solvent were used to prepare hydrogels in the absence of any chemical initiators and cross-linking agents. The solutions were injected into test tubes and then deaerated by bubbling with high-purity nitrogen to remove the dissolved oxygen. Then the solutions were directionally frozen over liquid nitrogen by using a self-made directional-freezing equipment with the freezing rates of 2, 5, 10 and 20 mm min^{-1}, respectively. The frozen HEMA solutions were irradiated with ^{60}Co γ-rays at a dose rate of 2.5 kGy/h and at a temperature of about −10 °C (ice−salt bath), ensuring the preservation of the solvent crystals. HEMA (m.p.: −12 °C) in the liquid state could be easily polymerized and cross-linked under γ-rays irradiation. It was found that the HEMA solutions transformed into hydrogels after only 1 h irradiation (2.5 kGy). To ensure the full conversion of HEMA, a total absorbed dose of 5.0 kGy was always applied for the hydrogel preparation. More detailed information on the radiation-induced polymerization and cross-linking of HEMA in the frozen state can be found in our previous study.[24] The organogels were immersed into a large excess of deionized water for 2 d with the change of water every 6 h to obtain PHEMA hydrogels.

Preparation of PHEMA/Ag Nanocomposite Hydrogels. The prepared PHEMA hydrogels were swollen to the same water content of 60 wt %. A small piece of hydrogel sample (0.28 g) cut into a cubic shape was soaked into an $AgNO_3$ aqueous solution (0.01, 0.02, 0.04, or 0.06 mol L^{-1}, 36 mL) for 48 h. Then the soaked hydrogel was dipped into a freshly prepared $NaBH_4$ solution (0.03, 0.06, 0.12, or 0.18 mol L^{-1}, 18 mL) for another 24 h to ensure the full reduction of silver ion into elemental silver. The resulting PHEMA/Ag nanocomposite hydrogel was thoroughly washed with deionized water and then kept in water for further use.

Scanning Electron Microscopy (SEM) Investigation. The middle part of the PHEMA gels were cut into strips and then plunged into liquid nitrogen for about 5 min. The frozen strips were subsequently freeze-dried in a FD2-1B-50 vacuum freeze-dryer (Beijing Boyikang Laboratory Apparatus Co. Ltd.) for about 24 h to remove the solvent completely, and then the dried samples were cracked in the direction parallel to the freezing direction. After being sputter-coated with platinum for 15 min, the morphologies of these fractured surfaces were observed with a Hitachi S-4800 cold field emission scanning electron microscope (Tokyo, Japan) with an accelerating voltage of 5 kV.

Transmission Electron Microscopy (TEM) Investigation. The Ag nanocomposite hydrogels were ground into microsized powders and then dispersed into water. The dispersions were coated on a copper grid and then dried in air. Transmission electron microscopy (TEM) observation of the Ag NPs was performed with a FEI TF20 instrument (FEI, USA) at an acceleration voltage of 200 kV. To understand the spatial distribution of the Ag NPs in the nanocomposite hydrogels, TEM observation was also performed on thin slices (80−100 nm) obtained via microtoming from freeze-dried specimens that were embedded with epoxy resin and cured for about 12 h at 60°. Microtoming was performed with a Leica EM UC 6 microtome (Leica, Germany) at a rate of 0.2−0.4 mm/s at room temperate.

The particle sizes of the Ag NPs were analyzed with the software Nano Measurer (version 1.2.0) by counting about 100 particles in several TEM images. The particles generally do not show regular shapes, so their sizes were evaluated by averaging the long and short diameters (or lengths).

X-ray Diffraction (XRD) Measurement. The Ag nanocomposite hydrogels ground into powders were used for XRD measurement. The spectra were recorded on a PANalytical-X'Pert PRO diffractometer (Cu radiation, λ = 1.5418 Å) running at 40 kV and 40 mA (PANalytical, Holland).

BET Surface Area Analysis. The Brunauer−Emmett−Teller (BET) specific surface areas of the gel samples cracked into small lumps were evaluated on the basis of nitrogen adsorption isotherms using a Quantachrome NOVA 2000e sorption analyzer (Quantachrome, USA) at liquid nitrogen temperature.

ICP-AES Analysis. The Ag nanoparticles in the composite hydrogels were reacted with concentrated HNO_3 to form water-soluble $AgNO_3$, and then the diluted aqueous $AgNO_3$ solutions were measured by inductively coupled plasma atomic emission spectroscopy (ICP-AES) on an SPECTRO ARCOS EOP instrument (SPECTRO Analytical Instruments GmbH, Germany).

Compressive Mechanical Tests. The cylinder-shaped specimens for compressive tests were with a height and a diameter of 5 and 13 mm, respectively. The specimens were tested with an Instron 3366 electronic universal testing machine (Instron Corporation, MA, USA) at a crosshead speed of 60% min^{-1} and a compressive ratio of 95%. To obtain reliable values, at least three parallel specimens were used for each test. Cyclic measurements were performed in immediate succession with the same specimen for 10 run cycles.

Catalytic Reduction of *o*-Nitroaniline. For the catalytic reduction of *o*-nitroaniline, *o*-nitroaniline (0.5 mL, 0.85 mmol L^{-1}) was added into the freshly prepared $NaBH_4$ solution (2 mL, 0.3 mol L^{-1}) and then a PHEMA/Ag nanocomposite hydrogel sample with a solid content of about 0.11 g was placed. The conversion of *o*-nitroaniline to 1,2-benzenediamine was monitored with a Shimadzu UV-2450 spectrophotometer (Shimadzu, Japan) over a scanning range of 250−500 nm at ambient temperature. The successive catalysis was performed by washing the gel sample and immersing into a large amount of deionized water for 2 h after each reaction, and then the gel sample was used again.

DOI: 10.1021/acssuschemeng.5b00482
ACS Sustainable Chem. Eng. 2015, 3, 1915−1924

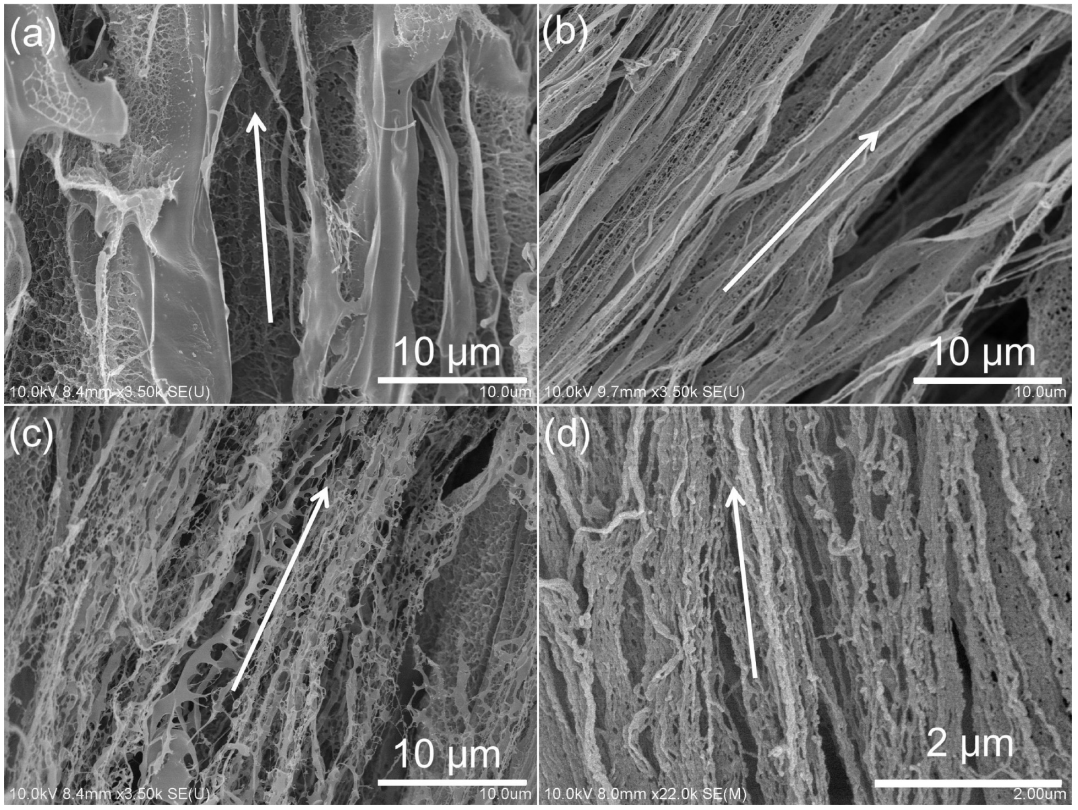

Figure 1. SEM images of the PHEMA hydrogels prepared with different freezing rates in the direction parallel to the freezing direction indicated with arrows. The freezing rates were 2 (a), 5 (b), 10 (c) and 20 (d) mm min^{-1}, respectively. HEMA concentration: 2 mol L^{-1}.

RESULTS AND DISCUSSION

Microstructures of PHEMA Gels. Both monomer concentration and freezing rate are important factors affecting the microstructures of the hydrogels. In this work, two series of PHEMA hydrogels were prepared by varying the monomer concentration or the freezing rate while keeping the other one constant.

First, we investigated the effect of freezing rate on the microstructures of the hydrogels. Figure 1 shows the SEM images of the middle part of the PHEMA hydrogels fabricated at a constant monomer concentration of 2 mol L^{-1} but varying freezing rates (from 2 to 20 mm min^{-1}). Generally, the hydrogels all show obvious anisotropic porous microstructures, with large (more than 10 μm) and long channels aligned along the freezing direction. At the low freezing rates of 2 and 5 mm min^{-1}, the pore walls are mainly continuous and dense and with a wall thickness of ca. 100−200 nm (Figure 1a,b). It is necessary to notice that many tiny pores (generally less than 1 μm) appear on the walls at the freezing rate of 5 mm min^{-1} (Figure 1b). When the freezing rate is increased to 10 mm min^{-1}, more and bigger (in micrometers) pores appear on the walls, and some regions even change into meshes consisted of nanowires (Figure 1c). With further increased freezing rate, most of the walls are transformed into nanowires (mostly with a diameter of 30−50 nm) mainly aligned along the freezing direction (Figure 1d).

Figure 2 shows the microstructures of the hydrogels prepared at the monomer concentrations from 1.0 to 3.0 mol L^{-1} at a constant freezing rate of 10 mm min^{-1}. The microstructure of the hydrogels changes dramatically with increasing monomer concentration. At a low monomer concentration of 1.0 mol L^{-1}, the hydrogel present an interesting porous mesh structure mainly constructed of nanowires (mostly <50 nm, Figure 2a) and some submicrometer or microsized nanowires (Figure 2b). With the increase of monomer concentration (1.5 and 2.0 mol L^{-1}), the morphology transforms into mesh structures constructed of nanowires connected by tiny microsized sheets (Figure 2c,d). And at the monomer concentrations of 2.5 and 3.0 mol L^{-1}, continuous and dense pore walls rather than nanowires are found (Figure 2e,f).

These observations suggest that a monomer concentration lower than 2.0 mol L^{-1} and a freezing rate higher than 10 mm min^{-1} are beneficial to the formation of nanowires in the gels. As the hydrogel prepared at a low monomer concentration usually has poorer mechanical properties, we chose the monomer concentration of 2.0 mol L^{-1} and the freezing rate of 20 mm min^{-1} to prepare hydrogels for further studies.

The microstructures of the PHEMA hydrogels prepared by using TBA as the solvent are quite different from those of the hydrogels prepared using water as the solvent,[24,31] as water usually forms microsized or even larger columnar or lamellar crystals rather than needle-like crystals of TBA during the directional freezing process. The phase separation induced by the crystallization of solvents during directional freezing has been well studied.[5,23,24,32] During the directional freezing of HEMA/TBA solution, needle crystals of TBA grow directionally from the bottom to the top of the solution, and the monomer molecules are expelled to fill the gaps among them. The increased freezing rate leads to an increased degree of supercooling and hence the formation of more tiny needle crystals, which prevent the formation of large aggregates of HEMA. Since the polymerization of monomer molecules is performed in the frozen state, the phase separation-induced

DOI: 10.1021/acssuschemeng.5b00482
ACS Sustainable Chem. Eng. 2015, 3, 1915−1924

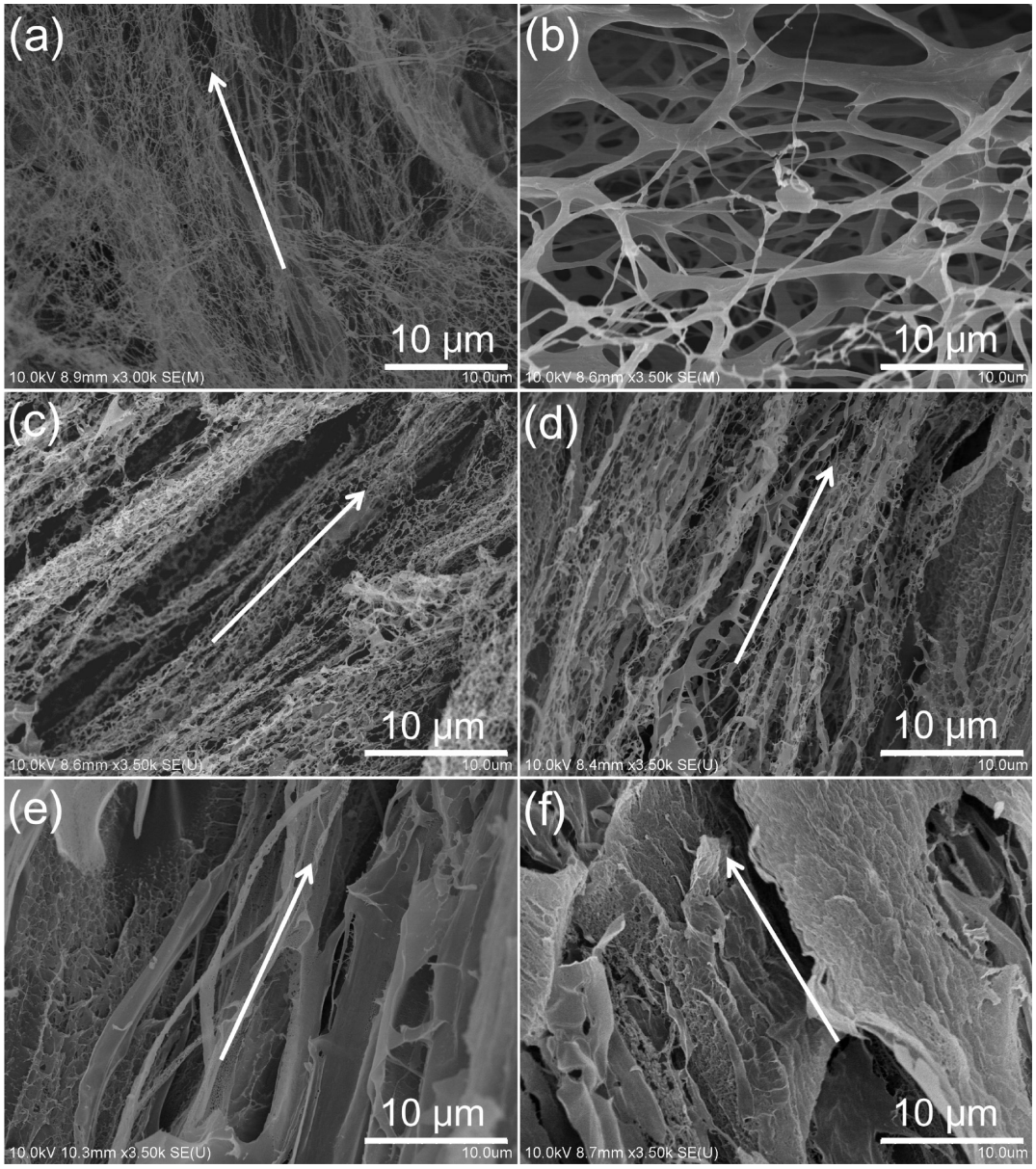

Figure 2. SEM images of the PHEMA hydrogels prepared with different monomer concentrations in the direction parallel to the freezing direction (indicated with arrows). The monomer concentrations are 1.0 (a, b), 1.5 (c), 2.0 (d), 2.5 (e) and 3.0 (f) mol L^{-1}, respectively. The freezing rate of all the hydrogels above is 10 mm min^{-1}.

microstructure can be preserved. Therefore, the hydrogels show the microstructure change from continuous and dense pore walls to meshes consisted of nanowires with the increasing rates.

The effect of monomer concentration on the microstructure can be explained as follows: The solution with a lower monomer concentration contains more TBA, and hence more TBA crystals are formed and grow along the freezing direction. The TBA crystals separate the HEMA molecules into many tiny domains aligned along the freezing direction, which transform into nanowires after the polymerization. On the contrary, at a higher monomer concentration, more HEMA molecules are easier to aggregate to form larger aligned structures, i.e., the continuous and dense pore walls.

Characterization of PHEMA/Ag NPs Composite Hydrogels. When $AgNO_3$ soaked in the PHEMA hydrogels is reduced with $NaBH_4$, elemental Ag is formed. Figure 3a–d shows the morphologies of the PHEMA/Ag nanocomposite hydrogels prepared with different $AgNO_3$ concentrations. With comparison to the original PHEMA hydrogels (Figure 1d and Figure 2a), some NPs are found on the nanowires in the composite hydrogels. The NPs should be the elemental Ag, as proven by the appearance of the Ag peaks in the EDX spectra (Figure S1). TEM observations performed with Ag nanocomposite hydrogels ground into microsized powders also prove the presence of Ag NPs in the composite hydrogels (Figure 3e–h).

TEM observations of Ag NPs were also performed with thin slices microtomed from the specimens along the freezing direction. As shown in Figure 4a–c, there is a spatial distribution of the Ag NPs, and they are mainly distributed along some lines. Together with the SEM images (Figure 3a–d), it is reasonable to conclude that the Ag NPs are formed and deposited on the directionally aligned nanowires. The NPs are

DOI: 10.1021/acssuschemeng.5b00482
ACS Sustainable Chem. Eng. 2015, 3, 1915–1924

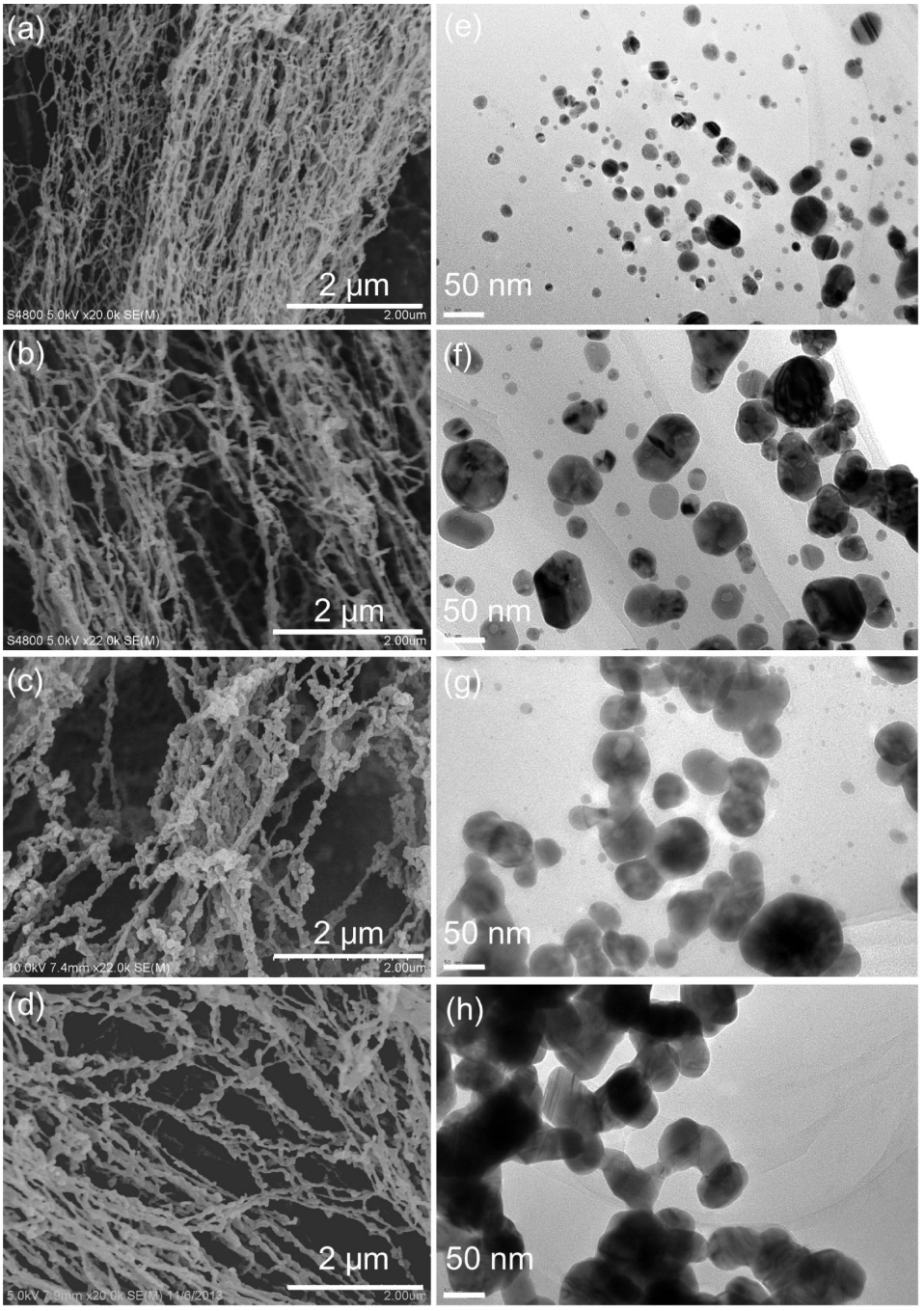

Figure 3. SEM and TEM images of the PHEMA/Ag nanocomposite hydrogels prepared with the $AgNO_3$ concentrations of 0.01 (a, e), 0.02 (b, f), 0.04 (c, g) and 0.06 mol L^{-1} (d, h), respectively. All the hydrogels were made with 2 mol L^{-1} HEMA solution and at the freezing rate of 20 mm min^{-1}.

generally separated rather than aggregated into clusters in the composite hydrogels, though there is some degree of aggregation for the NPs formed at a higher $AgNO_3$ concentration of 0.06 mol L^{-1} (Figure 4c).

To confirm that the NPs are nanocrystals, high-resolution TEM images were taken from a round and an elliptical Ag NPs, as shown in Figure 4d and Figure S2. They show the same lattice structure, with a lattice distance of approximately 0.24 nm, corresponding to the Ag (111) lattice plane,[33,34] which is the basal plane for Ag single crystals. The XRD patterns of the PHEMA/Ag nanocomposite hydrogels are shown in Figure 5. Except for the broad peaks centered around 18° attributed to the amorphous structure of PHEMA, all samples exhibit the typical crystalline peaks of the face centered cube structure of silver NPs (α = 4.09 Å, JCPDS No. 4-783), with 2θ values of 38.07° (111), 44.17° (200), 64.43° (220) and 77.37° (311).[35,36] The intensity of the diffraction peaks attributed to Ag NPs increase with the increase of $AgNO_3$ concentration. Both TEM and XRD characterizations prove the existence of Ag nanocrystals in the composite hydrogels.

The sizes of the Ag NPs prepared at different $AgNO_3$ concentrations were evaluated from TEM images and summarized in Figure 6a. The size of the Ag NPs increases with the increase of $AgNO_3$ concentration, from 16.5 ± 5.8 nm

DOI: 10.1021/acssuschemeng.5b00482
ACS Sustainable Chem. Eng. 2015, 3, 1915−1924

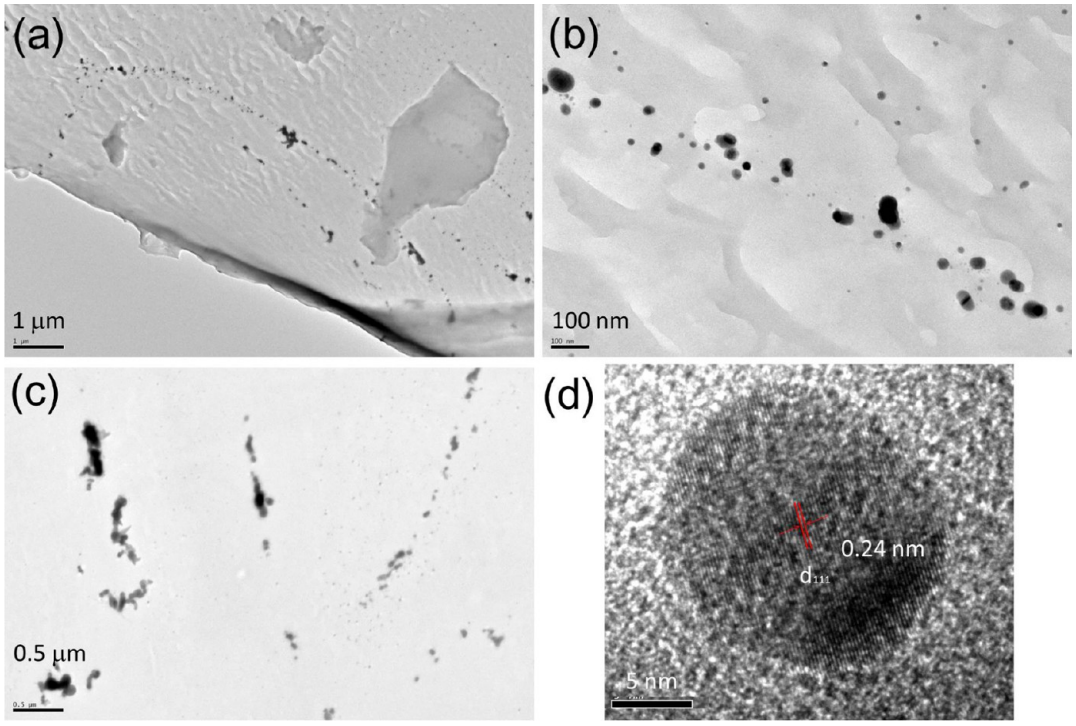

Figure 4. (a–c) TEM images of the PHEMA/Ag nanocomposite hydrogels prepared with the $AgNO_3$ concentrations of 0.04 (a, b) and 0.06 mol L^{-1} (c), and (d) the high-resolution TEM image of a round Ag nanoparticle. The hydrogel was made with 2 mol L^{-1} HEMA solution and at the freezing rate of 20 mm min^{-1}.

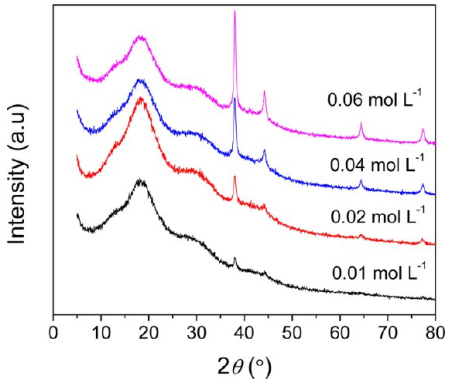

Figure 5. XRD patterns of the PHEMA/Ag nanocomposite hydrogels prepared with different $AgNO_3$ concentrations. All the hydrogels were made with 2.0 mol L^{-1} HEMA solution and the freezing rate was 20 mm min^{-1}.

at the concentration of 0.01 mol L^{-1} to 58.4 ± 11.6 nm at 0.06 mol L^{-1}. The Ag contents in the dried hydrogels measured by ICP-AES are 0.13, 0.30, 0.67 and 1.27%, respectively (Figure 6b). Both size and content of Ag NPs in the hydrogels increase with increasing $AgNO_3$ concentration, in consistent with the SEM and TEM observations.

The Ag contents in the composite hydrogels prepared with different freezing rates and monomer concentrations are very similar (ca. 0.13–0.15%) when the $AgNO_3$ concentration is the same (0.01 mol L^{-1}).

Compressive Mechanical Properties of the Hydrogels. The PHEMA and PHEMA/Ag nanocomposite hydrogels all possess very good compressive mechanical properties. Figure 7a shows that the compressive stresses (σ_c) are mostly more than 1 MPa at a compressive strain (ε_c) of 95%. The σ_c of the hydrogels significantly decreases with increasing freezing rates, from 6.6 MPa at the freezing rate of 2 mm min^{-1} to 0.4 MPa at 20 mm min^{-1}. In addition, at the same freezing rate the σ_c of the PHEMA/Ag nanocomposite hydrogel is slightly higher than that of the corresponding PHEMA hydrogel, suggesting the formation of complexation between the Ag NPs and the network of hydrogels. The cyclic compressive σ_c–ε_c curves for 10 runs shows small deviations from the prior ones, especially for the hydrogels prepared at the low freezing rates (Figure 7b and Figure S3), suggesting the excellent deformation recovery of the PHEMA/Ag nanocomposite hydrogels. The high compressive stresses and excellent deformation recovery provide the PHEMA/Ag nanocomposite hydrogels with excellent reusability.

Catalytic Performance. To evaluate the catalytic properties of the obtained Ag NPs composite hydrogels, the reduction reaction of *o*-nitroaniline to 1,2-benzenediamine by sodium borohydride was investigated.[37,38] The absorbance at 412 nm of *o*-nitroaniline in the UV/vis spectra was employed to monitor the reaction progress as a function of time.

Figure 8a shows the UV/vis spectra for the reduction of *o*-nitroaniline at different reaction times. Without the addition of a PHEMA/Ag nanocomposite hydrogel into the solution, the absorbance at 412 nm is almost unchanged within 3 h, suggesting that the reduction does not proceed in the absence of a catalyst. But when a PHEMA/Ag nanocomposite hydrogel is added, the absorbance at 412 nm decreases gradually to nearly 0 after about 20 min, accompanying the color of the solution changing from yellow to colorless (see the inset photos in Figure 8a). The full conversion of *o*-nitroaniline to 1,2-benzenediamine is also proven by FTIR and HNMR characterization of the reactant and the product (Figure S4 and Figure S5).

DOI: 10.1021/acssuschemeng.5b00482
ACS Sustainable Chem. Eng. 2015, 3, 1915–1924

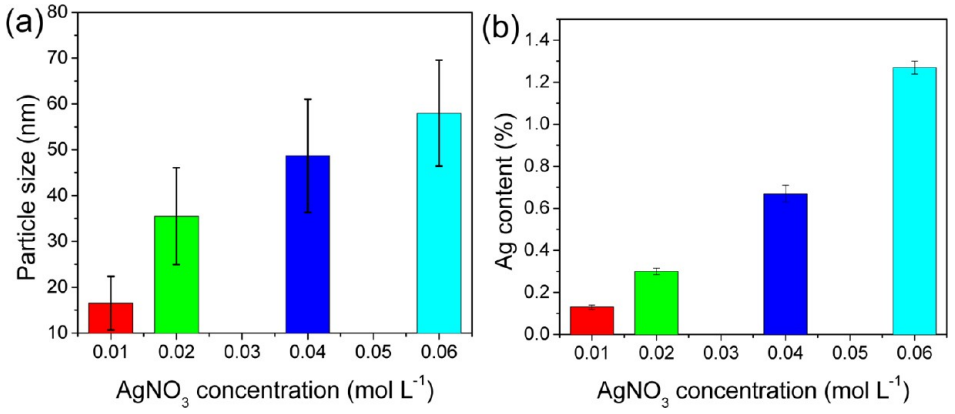

Figure 6. Sizes (a) and contents (b) of the Ag NPs prepared with different $AgNO_3$ concentrations.

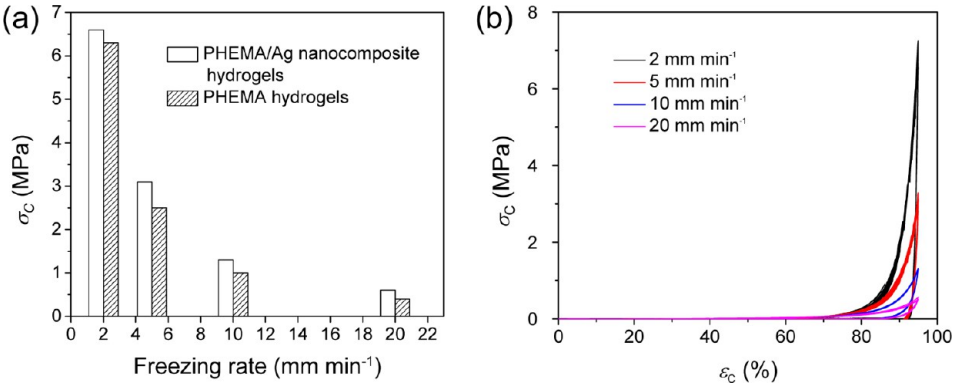

Figure 7. Compressive mechanical performances of the hydrogels prepared with different freezing rates. The compressive strengths (σ_c, ε_c = 95%) of the PHEMA and PHEMA/Ag nanocomposite hydrogels (a), and the cyclic compressive σ_c–ε_c curves of the PHEMA/Ag nanocomposite hydrogels (b). All the hydrogels were made with 2.0 mol L^{-1} HEMA solution, and the PHEMA/Ag nanocomposite hydrogels were prepared with 0.01 mol L^{-1} $AgNO_3$ solution.

Because the concentration of $NaBH_4$ is in large excess to that of *o*-nitroaniline, the first-order rate kinetics can be applied to the reaction with consideration to the concentration of *o*-nitroaniline only.[39−42] Therefore, the reaction kinetic can be described as

$$-d_C/d_t = k_{app}C_t \quad (1)$$

where C_t is the concentration of *o*-nitroaniline at time *t* and k_{app} is the apparent rate constant of the reaction.

As shown in Figure 8b, a linear $\ln(C_t/C_0) \sim t$ relationship can be observed with 10 cycles, suggesting that the reaction follows first-order kinetics as discussed above. The k_{app} can be obtained from the slope of the linear line directly, and it is 0.165 min^{-1} for the first time. The hydrogel was washed with water and then was used to catalyze the reduction reaction for 9 times. Figure 8c shows that the k_{app} value decreases gradually in the following three times, and they are 0.150, 0.136 and 0.127 min^{-1}, respectively; however, an unexpected increase in k_{app} is found from 5 to 9 times. The possible reason for the increase is that the more cracks (not into pieces) are shown in the hydrogel sample with the increase of cycle number, leading to the faster contact of reactants with the Ag NPs. It is worth to note that no detectable Ag NPs leaked from the nanocomposite hydrogels into the reacted solution even after 10 cycles.

The catalysis performance of the Ag NPs nanocomposite hydrogels should be affected by the microstructures of the hydrogels and the morphologies of the Ag NPs, etc. It is known that a higher freezing rate and a lower monomer concentration are beneficial to the formation of nanowires in the hydrogels, which provide larger specific surface area for the formation and deposition of well-dispersed Ag NPs. We compared the k_{app} values of the catalytic reduction of *o*-nitroaniline with the specific surface areas of the hydrogels prepared at different freezing rates and monomer concentrations. The k_{app} value and the specific surface area both increase with increasing freezing rate (Figure 9a), whereas they decrease as monomer concentration increases (Figure 9b), showing a direct correlation between the k_{app} and the specific surface areas of the hydrogels. In addition, the more porous microstructure of the hydrogel prepared at a lower monomer concentration allows the easier and faster diffusion of reactants to the catalysts. Therefore, the Ag NPs nanocomposite hydrogels prepared at a higher freezing rate and/or a lower monomer concentration exhibit better catalysis performance.

For the reactions catalyzed with the composite hydrogels prepared with different $AgNO_3$ concentrations, their k_{app} value first decreases and then increases with increasing $AgNO_3$ concentration (Figure 9c). $AgNO_3$ concentration affects the morphology and content of Ag NPs in the composite hydrogels. As shown in Figures 3 and 6, the Ag NPs formed at $AgNO_3$ concentration of 0.01 mol L^{-1} are the smallest (16 nm) and are separately distributed, so their large specific surface area provides more catalytic active sites and hence higher catalytic activity. Although the content of Ag NPs increases with increasing $AgNO_3$ concentration, their smaller specific surface area due to the increase of particle size lowers

DOI: 10.1021/acssuschemeng.5b00482
ACS Sustainable Chem. Eng. 2015, 3, 1915−1924

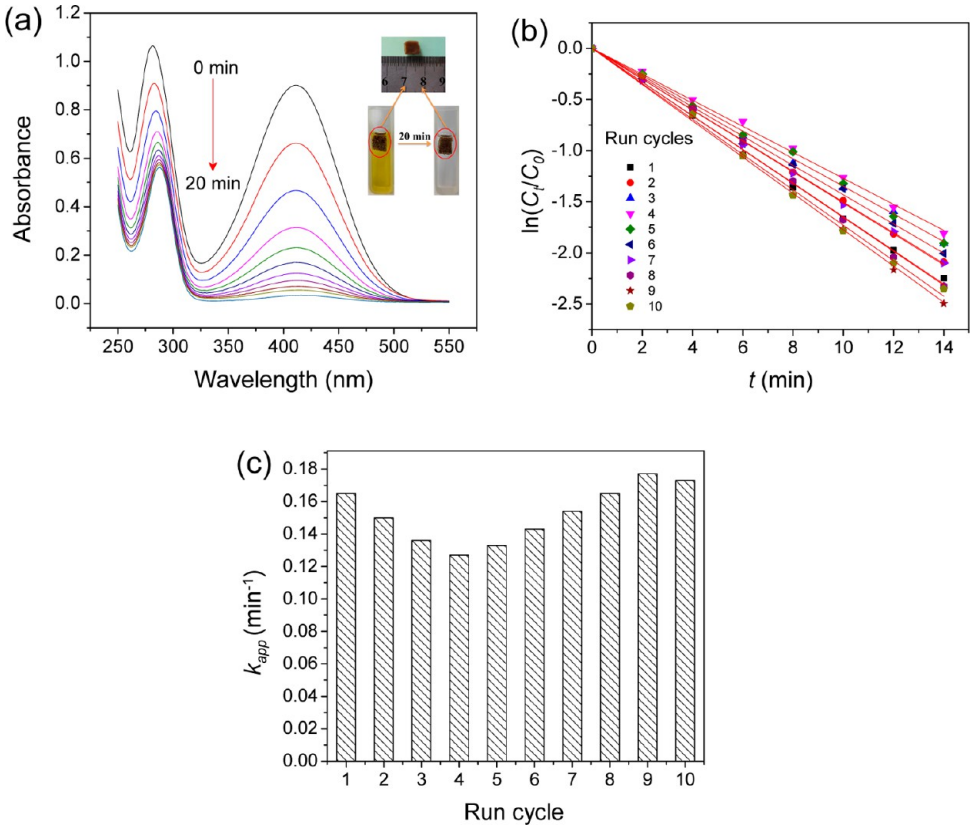

Figure 8. Catalytic activity of PHEMA/Ag nanocomposite hydrogels prepared with 0.01 mol L^{-1} $AgNO_3$ concentration. (a) Successive UV/vis spectra of the aqueous solution of *o*-nitroaniline and $NaBH_4$ in the presence of a PHEMA/Ag composite hydrogel; (b) the $\ln(C_t/C_0) \sim t$ plots and (c) the corresponding k_{app} values for 10 successive catalysis run cycles.

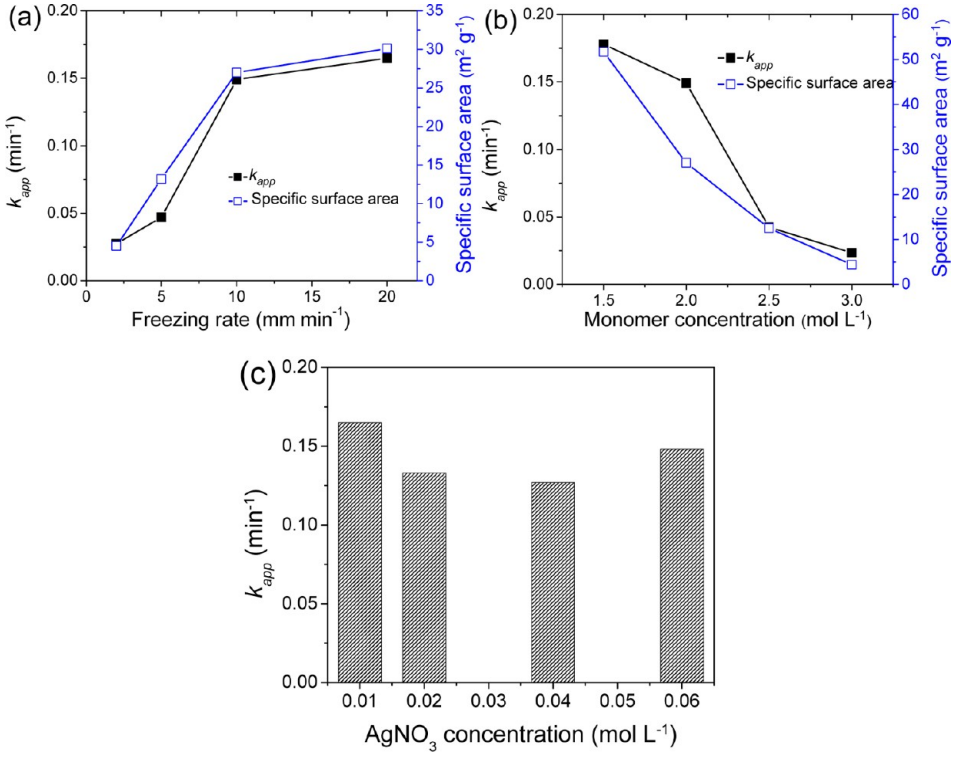

Figure 9. Factors affecting the catalysis performance of the Ag NPs nanocomposite hydrogels. The apparent rate constants (k_{app}) of the composite hydrogels prepared at different freezing rates (a), monomer concentrations (b) and $AgNO_3$ concentrations (c), with the other two factors kept constant. The specific surface areas of the PHEMA hydrogels are included in (a) and (b). The monomer concentration was 2.0 mol L^{-1} (a, c), the $AgNO_3$ concentration was 0.01 mol L^{-1} (a, b), and the freezing rate was 10 mm min^{-1} (b) and 20 mm min^{-1} (c).

DOI: 10.1021/acssuschemeng.5b00482
ACS Sustainable Chem. Eng. 2015, 3, 1915−1924

their catalytic activity. The decrease in specific surface area becomes less significant with the further increase in the size of NPs, and hence the increase of the amounts of Ag NPs makes a more important contribution to the catalytic activity. This might be the main reason for the slightly increased k_{app} value for the composite hydrogel prepared at the $AgNO_3$ concentration of 0.06 mol L^{-1}.

CONCLUSIONS

In summary, aligned nanowire structured PHEMA hydrogels have been prepared by directional freezing and γ-radiation initiated polymerization using TBA as the solvent. By observing the microstructures of the hydrogels prepared under different conditions, it is concluded that an enhanced freezing rate and a lower monomer concentration are more beneficial to the formation of nanowire hydrogels. Silver NPs are easily introduced into the hydrogels, and they are formed and deposited on the directionally aligned polymeric nanowires. The PHEMA/Ag NPs composite hydrogels show excellent catalytic properties and reusability. We postulate that more hydrogels or other polymeric materials with different microstructures can be prepared with the DF and a polymerization method by using other monomers and solvents. In addition, other metal nanoparticles can also be introduced into the hydrogels for more applications in various fields.

ASSOCIATED CONTENT

Supporting Information

The Supporting Information is available free of charge on the ACS Publications website at DOI: 10.1021/acssuschemeng.5b00482.

EDS spectra of the PHEMA/Ag nanocomposite hydrogels (Figure S1), high-resolution TEM image of an elliptical Ag nanoparticle (Figure S2), TGA curves of the dried hydrogels (Figure S3), the cyclic compressive σ_c−ε_c curves of the PHEMA/Ag nanocomposite hydrogels (Figure S4), and FTIR and ^{1}H NMR spectra of *o*-nitroaniline and 1,2-benzenediamine (Figure S5 and Figure S6) (PDF)

AUTHOR INFORMATION

Corresponding Author

*H. Wang. E-mail: wanghl@bnu.edu.cn.

Notes

The authors declare no competing financial interest.

ACKNOWLEDGMENTS

The authors appreciate financial support from the National Science Foundation of China (Grant No. 21274013), the Fundamental Research Funds for the Central Universities and the Program for Changjiang Scholars and Innovative Research Team in University (PCSIRT). Dr. Zhiyong Li from Chemistry Institute, Chinese Academy of Sciences is acknowledged for helping us with the microtomy.

REFERENCES

(1) Zhang, X.; Yang, Y.; Yao, J.; Shao, Z.; Chen, X. Strong collagen hydrogels by oxidized dextran modification. *ACS Sustainable Chem. Eng.* **2014**, *2*, 1318−1324.

(2) Kim, Y.; Abuelfilat, A. Y.; Hoo, S. P.; Al-Abboodi, A.; Liu, B.; Ng, T.; Chan, P.; Fu, J. Tuning the surface properties of hydrogel at the nanoscale with focused ion irradiation. *Soft Matter* **2014**, *10*, 8448−8456.

(3) Sato, R.; Kawakami, T.; Tokuyama, H. Preparation of polymeric macroporous hydrogels for the immobilization of enzymes using an emulsion-gelation method. *React. Funct. Polym.* **2014**, *76*, 8−12.

(4) Gil, E. S.; Park, S.-H.; Tien, L. W.; Trimmer, B.; Hudson, S. M.; Kaplan, D. L. Mechanically robust, rapidly actuating, and biologically functionalized macroporous poly(*N*-isopropylacrylamide)/silk hybrid hydrogels. *Langmuir* **2010**, *26*, 15614−15624.

(5) Barrow, M.; Zhang, H. Aligned porous stimuli-responsive hydrogels via directional freezing and frozen UV initiated polymerization. *Soft Matter* **2013**, *9*, 2723−2729.

(6) Zhang, H. F.; Hussain, I.; Brust, M.; Butler, M. F.; Rannard, S. P.; Cooper, A. I. Aligned two- and three-dimensional structures by directional freezing of polymers and nanoparticles. *Nat. Mater.* **2005**, *4*, 787−793.

(7) Zhao, D.; Zhu, J.; Zhu, Z.; Song, G.; Wang, H. Anisotropic hierarchical porous hydrogels with unique water loss/absorption and mechanical properties. *RSC Adv.* **2014**, *4*, 30308−30314.

(8) Jung, S. M.; Jung, H. Y.; Fang, W.; Dresselhaus, M. S.; Kong, J. A facile methodology for the production of in situ inorganic nanowire hydrogels/aerogels. *Nano Lett.* **2014**, *14*, 1810−1817.

(9) Ko, H.; Zhang, Z.; Chueh, Y.-L.; Saiz, E.; Javey, A. Thermoresponsive chemical connectors based on hybrid nanowire forests. *Angew. Chem., Int. Ed.* **2010**, *49*, 616−619.

(10) Im, J. S.; Bai, B. C.; In, S. J.; Lee, Y.-S. Improved photodegradation properties and kinetic models of a solar-light-responsive photocatalyst when incorporated into electrospun hydrogel fibers. *J. Colloid Interface Sci.* **2010**, *346*, 216−221.

(11) Liu, P.; Jiang, L.; Zhu, L.; Wang, A. Attapulgite/poly(acrylic acid) nanocomposite (ATP/PAA) hydrogels with multifunctionalized attapulgite (org-ATP) nanorods as unique cross-linker: preparation optimization and selective adsorption of Pb(II) ion. *ACS Sustainable Chem. Eng.* **2014**, *2*, 643−651.

(12) Zhu, J.; Wang, X.; He, C.; Wang, H. Mechanical properties, anisotropic swelling behaviours and structures of jellyfish mesogloea. *J. Mech. Behav. Biomed. Mater.* **2012**, *6*, 63−73.

(13) Wang, X.; Wang, H.; Brown, H. R. Jellyfish gel and its hybrid hydrogels with high mechanical strength. *Soft Matter* **2011**, *7*, 211−219.

(14) Chen, Y.; Wang, H. Jellyfish mesoglea as a matrix for the synthesis of extremely high content silver dendrites. *J. Colloid Interface Sci.* **2015**, *454*, 14−19.

(15) Ji, L.; Wang, Z.; Li, Z.; Liang, J. Preparation of aligned titania nanowires with an aligned carbon nanotube composite template. *Mater. Lett.* **2008**, *62*, 1979−1982.

(16) Vidyadharan, B.; Aziz, R. A.; Misnon, I. I.; Anil Kumar, G. M.; Ismail, J.; Yusoff, M. M.; Jose, R. High energy and power density asymmetric supercapacitors using electrospun cobalt oxide nanowire anode. *J. Power Sources* **2014**, *270*, 526−535.

(17) Han, S. W.; Lee, S.; Hong, J.; Jang, E.; Lee, T.; Koh, W.-G. Mutiscale substrates based on hydrogel-incorporated silicon nanowires for protein patterning and microarray-based immunoassays. *Biosens. Bioelectron.* **2013**, *45*, 129−135.

(18) Lin, B. F.; Megley, K. A.; Viswanathan, N.; Krogstad, D. V.; Drews, L. B.; Kade, M. J.; Qian, Y.; Tirrell, M. V. pH-responsive branched peptide amphiphile hydrogel designed for applications in regenerative medicine with potential as injectable tissue scaffolds. *J. Mater. Chem.* **2012**, *22*, 19447−19454.

(19) Yang, Z. Z.; Niu, Z. W. Binary hydrogel nanowires of invertible core/shell phases prepared in porous alumina membranes. *Chem. Commun.* **2002**, 1972−1973.

(20) Zhang, L.; Zhao, J.; Zhu, J.; He, C.; Wang, H. Anisotropic tough poly(vinyl alcohol) hydrogels. *Soft Matter* **2012**, *8*, 10439−10447.

(21) Romeo, H. E.; Hoppe, C. E.; Lopez-Quintela, M. A.; Williams, R. J. J.; Minaberry, Y.; Jobbagy, M. Directional freezing of liquid crystalline systems: from silver nanowire/PVA aqueous dispersions to highly ordered and electrically conductive macroporous scaffolds. *J. Mater. Chem.* **2012**, *22*, 9195−9201.

DOI: 10.1021/acssuschemeng.5b00482
ACS Sustainable Chem. Eng. 2015, 3, 1915−1924

(22) He, H.; Zhang, D.; Xu, X. Electrically conductive multiwall carbon nanotubes/poly(vinyl alcohol) composites with aligned porous morphologies. *J. Macromol. Sci., Part B: Phys.* **2012**, *51*, 2493−2498.
(23) Okaji, R.; Taki, K.; Nagamine, S.; Ohshima, M. Preparation of porous honeycomb monolith from UV-curable monomer/dioxane solution via unidirectional freezing and UV irradiation. *J. Appl. Polym. Sci.* **2012**, *125*, 2874−2881.
(24) Chen, M.; Zhu, J.; Qi, G.; He, C.; Wang, H. Anisotropic hydrogels fabricated with directional freezing and radiation-induced polymerization and crosslinking method. *Mater. Lett.* **2012**, *89*, 104−107.
(25) Barrow, M.; Eltmimi, A.; Ahmed, A.; Myers, P.; Zhang, H. Frozen polymerization for aligned porous structures with enhanced mechanical stability, conductivity, and as stationary phase for HPLC. *J. Mater. Chem.* **2012**, *22*, 11615−11620.
(26) Okaji, R.; Taki, K.; Nagamine, S.; Ohshima, M. Preparation of a unique, multihollow-core honeycomb structure via the unidirectional freezing of a binary solvent system. *J. Appl. Polym. Sci.* **2013**, *130*, 526−534.
(27) Akahori, H.; Ishii, H.; Nonaka, I.; Yoshida, H. A simple freeze-drying device using tert-butyl alcohol for SEM specimens. *J. Electron Microsc.* **1988**, *37*, 351−352.
(28) Qian, F.; Ni, N.; Chen, J.-W.; Desikan, S.; Naringrekar, V.; Hussain, M. A.; Barbour, N. P.; Smith, R. L. Formation of zinc-peptide spherical microparticles during lyophilization from tert-butyl alcohol/water co-solvent system. *Pharm. Res.* **2008**, *25*, 2799−2806.
(29) van der Schoot, S. C.; Nuijen, B.; Flesch, F. M.; Gore, A.; Mirejovsky, D.; Lenaz, L.; Beijnen, J. H. Development of a bladder instillation of the indoloquinone anticancer agent EO-9 using tert-butyl alcohol as lyophilization vehicle. *AAPS PharmSciTech* **2007**, *8*, E78−E87.
(30) Fabietti, L. M.; Trivedi, R. Development of interface morphologies in the tert butyl alcohol-water system. *J. Cryst. Growth* **1997**, *182*, 185−197.
(31) Zhu, J.; Wang, J.; Liu, Q.; Liu, Y.; Wang, L.; He, C.; Wang, H. Anisotropic tough poly(2-hydroxyethyl methacrylate) hydrogels fabricated by directional freezing redox polymerization. *J. Mater. Chem. B* **2013**, *1*, 978−986.
(32) Zhang, H.; Cooper, A. I. Aligned porous structures by directional freezing. *Adv. Mater.* **2007**, *19*, 1529−1533.
(33) Chen, G.; Si, X.; Yu, J.; Bai, H.; Zhang, X. Doping nano-Co_3O_4 surface with bigger nanosized Ag and its photocatalytic properties for visible light photodegradation of organic dyes. *Appl. Surf. Sci.* **2015**, *330*, 191−199.
(34) Viana, M. M.; Mohallem, N. D. S.; Miquita, D. R.; Balzuweit, K.; Silva-Pinto, E. Preparation of amorphous and crystalline Ag/TiO_2 nanocomposite thin films. *Appl. Surf. Sci.* **2013**, *265* (0), 130−136.
(35) Zheng, Y.; Wang, A. Ag nanoparticle-entrapped hydrogel as promising material for catalytic reduction of organic dyes. *J. Mater. Chem.* **2012**, *22* (32), 16552−16559.
(36) Kulkarni, A. A.; Bhanage, B. M. Ag@AgCl nanomaterial synthesis using sugar cane juice and its application in degradation of azo dyes. *ACS Sustainable Chem. Eng.* **2014**, *2* (4), 1007−1013.
(37) Chadha, R.; Das, A.; Maiti, N.; Kapoor, S. Synthesis of silver nanoparticles: Effects of anionic ligands on formation and catalytic activity. *Mater. Chem. Phys.* **2014**, *148*, 1124−1130.
(38) Celen, B.; Ekiz, D.; Piskin, E.; Demirel, G. Green catalysts based on bio-inspired polymer coatings and electroless plating of silver nanoparticles. *J. Mol. Catal. A: Chem.* **2011**, *350*, 97−102.
(39) Sharma, R. K.; Monga, Y.; Puri, A. Magnetically separable silica@Fe_3O_4 core-shell supported nano-structured copper(II) composites as a versatile catalyst for the reduction of nitroarenes in aqueous medium at room temperature. *J. Mol. Catal. A: Chem.* **2014**, *393*, 84−95.
(40) Zeng, T.; Zhang, X.-L.; Niu, H.-Y.; Ma, Y.-R.; Li, W.-H.; Cai, Y.-Q. In situ growth of gold nanoparticles onto polydopamine-encapsulated magnetic microspheres for catalytic reduction of nitrobenzene. *Appl. Catal., B* **2013**, *134*−*135*, 26−33.
(41) Zhu, C.-H.; Hai, Z.-B.; Cui, C.-H.; Li, H.-H.; Chen, J.-F.; Yu, S.-H. In situ controlled synthesis of thermosensitive poly(*N*-isopropylacrylamide)/Au nanocomposite hydrogels by gamma radiation for catalytic application. *Small* **2012**, *8*, 930−936.
(42) Li, S.; Ge, Y.; Tiwari, A.; Cao, S. A temperature-responsive nanoreactor. *Small* **2010**, *6*, 2453−2459.

DOI: 10.1021/acssuschemeng.5b00482
ACS Sustainable Chem. Eng. 2015, 3, 1915−1924